



Diode-pumped continuous-wave a- and c-cut Pr:Sr_{0.5}La_{0.5}Mg_{0.5}Al_{11.5}O₁₉ (Pr:ASL) visible lasers at 645 and 726 nm



Shidong Zhou^a, Yuxin Pan^a, Jian Liu^a, Qingsong Song^a, Jie Xu^a, Dongzhen Li^a, Peng Liu^a, Xiaodong Xu^{a,*}, Bin Xu^b, Jun Xu^{c,**}, Ivan Buchvarov^d, Kheirreddine Lebbou^e

^a Jiangsu Key Laboratory of Advanced Laser Materials and Devices, School of Physics and Electronic Engineering, Jiangsu Normal University, Xuzhou, 221116, China

^b Department of Electronic Engineering, Xiamen University, Xiamen, 361005, China

^c School of Physics Science and Engineering, Institute for Advanced Study, Tongji University, Shanghai, 200092, China

^d Department of Physics, Sofia University, 5 James Bourchier Blvd., 1164, Sofia, Bulgaria

^e Institut Lumière Matière, UMR5306 Université Lyon1-CNRS, Université de Lyon, Lyon, 69622, Villeurbanne Cedex, France

ARTICLE INFO

Article history:

Received 22 January 2019

Received in revised form

9 April 2019

Accepted 11 April 2019

Available online 12 April 2019

Keywords:

Pr:ASL

Czochralski method

Spectral property

Laser property

ABSTRACT

Pr³⁺-doped Sr_{0.5}La_{0.5}Mg_{0.5}Al_{11.5}O₁₉ (ASL) crystal along ⟨100⟩ direction was successfully grown using the Czochralski technique under azote atmosphere. Absorption and emission spectra of Pr:ASL crystal have been measured at room temperature. Continuous-wave laser operation of the a-cut and c-cut Pr:ASL samples under InGaN laser diode pumping has been demonstrated. For deep red laser operation at about 726 nm, the maximum output powers achieved from a-cut sample was 92.8 mW with slope efficiency of about 11.9%, while 46.6 mW with slope efficiency of 8.0% for the c-cut sample. For red laser at about 645 nm, maximum output powers of 49.2 mW and 42.8 mW were obtained for the a-cut sample and c-cut sample, corresponding to a slope efficiency of 6.7% and 8.5%, respectively.

© 2019 Elsevier B.V. All rights reserved.

1. Introduction

During the past decades, solid-state laser sources, especially diode-pumped solid-state laser sources (DPSSL), have been greatly developed because their advantages, e.g. efficiency, compactness, maintenance and robustness, have attracted researchers working on them. Based on DPSSL technology, laser sources operating in visible wavelength range have been frequently investigated. These visible sources are indeed very applicable in color display, data storage and medical imaging [1–4]. Nonlinear frequency conversion is one of the main techniques to produce visible laser operation under the precondition of having near infrared fundamental waves, mostly based on Nd³⁺ ions [5]. Although the visible output power could be high because of the commercially available high-power 800-nm diode laser pump sources, the aforementioned advantages of DPSSLs have been destroyed more or less.

The development of InGaN diode laser has stimulated interest in

rare earth doped solid state materials to be used as visible media. Trivalent praseodymium (Pr³⁺) ion is one of the most promising candidates owing to its plentiful transition lines in the visible region [6,7]. The spectroscopic properties of Pr³⁺ ions in various hosts, such as single crystals [8,9], transparent ceramics [10], and glasses [11,12] have been investigated for exploring new laser media.

Pr³⁺-doped fluoride crystals have demonstrated efficient laser performance because of their relatively low phonon energies and comparably low crystal field strength, which reduces the non-radiative decay of the ³P₀ level to ¹D₂ level and excited state absorption to the 4f5d configuration [1]. During the last decade, laser oscillations in Pr:YLF (LiYF₄) [13,14], Pr:KY₃F₁₀ [15,16], Pr:BYF (BaY₂F₈) [17], Pr:LLF (LiLuF₄) [15,18], Pr:GLF (GdLiF₄) [19], Pr:KYF₄ [20], Pr:BYLF (Ba(Y_{0.8}Lu_{0.2})₂F₈) [21], and Pr,Gd:CaF₂ [22] crystals have been reported. As we know, compared with fluorides [23,24], oxide crystals have better mechanical properties and can be easily grown by the Czochralski method. Unfortunately, many Pr³⁺-doped oxide crystals possess a higher maximum phonon energy and stronger crystal field. So Pr³⁺-doped oxides lasers have been much less reported, except Pr:YAP [25,26], Pr,Mg:SrAl₁₂O₁₉ (SRA) [27,28],

* Corresponding author.

** Corresponding author.

E-mail addresses: xdxu79@jsnu.edu.cn (X. Xu), xujun@mail.shcnc.ac.cn (J. Xu).

Pr,Mg:CaAl₁₂O₁₉ [29], LaMgAl₁₁O₁₉ (LMA) [30], and Pr:Sr_{0.7}La_{0.3}Mg_{0.3}Al_{11.7}O₁₉ (ASL) [31].

SRA is a hexagonal aluminate with a magnetoplumbite structure and the space group $P6_3/mmc$ [32,33]. ASL and LMA crystal can be considered as a partially or, fully La-doped SRA crystal. The La³⁺ ions substitute the large divalent Sr²⁺ cationic sites and charge compensation will be accomplished by codoping with Mg²⁺ ions on the Al³⁺ sites [34,35]. These host materials have a relatively weak crystal field, which will benefit the laser operation of Pr³⁺ ions. In the past few years, some progress had been made based on rare earth doped SRA, LMA and ASL crystals. By using Sm,Mg:SRA crystal as active medium, laser oscillation was achieved in the orange at 593 nm and deep red at 648 nm with maximum output powers of 7 mW and 45 mW [36]. Continuous-wave laser operation of a Nd:LMA crystal was demonstrated at 1055 nm with a maximum output power of 1.71 W and slope efficiency of 40.4% [37]. Laser operation of Pr:LMA crystal pumped by a 444 nm blue diode laser was demonstrated in the red at 645 nm and deep red at 725 nm with maximum output powers of 16 mW and 30 mW [30]. Satayaporn et al. reported the visible laser performance of Pr:Sr_{1-x}La_xMg_xAl_{12-x}O₁₉ (x = 0.3) crystal [31], which combines the excellent radiative properties of SRA with the appropriate melting behavior of LMA in a solid solution Sr_{0.7}La_{0.3}Mg_{0.3}Al_{11.7}O₁₉. However, to operate the lasers some authors [29,31] used costly, cumbersome and not easily available 2 ω -OPSL as pump source instead of far more commonly used blue diode laser. Moreover, different La³⁺ composition in Pr:ASL crystal will change the crystal field environment of the host, which will lead to small change of spectral and laser properties of occupying Pr³⁺.

In this work, Pr³⁺-doped Sr_{0.5}La_{0.5}Mg_{0.5}Al_{11.5}O₁₉ (Pr:ASL) crystal has been successfully grown for visible laser generation. Using a standard blue diode laser as pump source, laser emissions at red and deep red were obtained. Moreover, by adjusting the x value in Sr_{1-x}La_xMg_xAl_{12-x}O₁₉ to be 0.5, we have interestingly found laser wavelength shifts from 643 nm to 645 nm and 725 nm to 726 nm compared with Pr:Sr_{0.7}La_{0.3}Mg_{0.3}Al_{11.7}O₁₉ crystal achieved in Ref. [31].

2. Crystal growth

Pr:ASL crystal is formed by replacement of Sr²⁺ ions by Pr³⁺ and La³⁺ in the uniaxial magnetoplumbite-type structure of strontium hexaaluminate, SrAl₁₂O₁₉ (space group $P6_3/mmc$), and charge compensation is achieved by substituting Mg²⁺ for Al³⁺. On the basis of laser experiments previously performed on Pr:SrAl₁₂O₁₉ crystals [27], the Pr³⁺ concentration of 3 at.% has been selected in Sr_{0.5}La_{0.5}Mg_{0.5}Al_{11.5}O₁₉ crystal. The crystal was grown along the <100> crystal orientation using the Czochralski method. Raw materials of Pr₆O₁₁, SrCO₃, La₂O₃, MgO and Al₂O₃ with 5 N purity were weighted, mixed, pressed and sintered at 1300 °C for 24 h. Then, the polycrystalline materials were loaded into an iridium crucible of 70 mm diameter and 45 mm height for crystal growth. During the growth the pulling rate was 0.8 mm/h, the rotation rate was 10–30 rpm, and the growth atmosphere was nitrogen. After growth, the crystal was cooled down to room temperature at a speed of 20–40 °C/h. Finally Pr:ASL crystal was obtained and had a size of 28 mm in diameter and 40 mm in length. The crystal cracking happened along the (001) cleavage plane during the crystal growth. Fig. 1 shows the polished Pr:ASL samples for laser experiments. The crystals were greenish and no inclusions and bubbles were observed in the samples.

The sample for spectroscopic measurements was cut from the crystal and two surfaces of the sample perpendicular to the (100) axis were optically polished with the thickness of about 1 mm. The Pr³⁺ concentration of the sample was 0.69×10^{20} ions/cm³. The

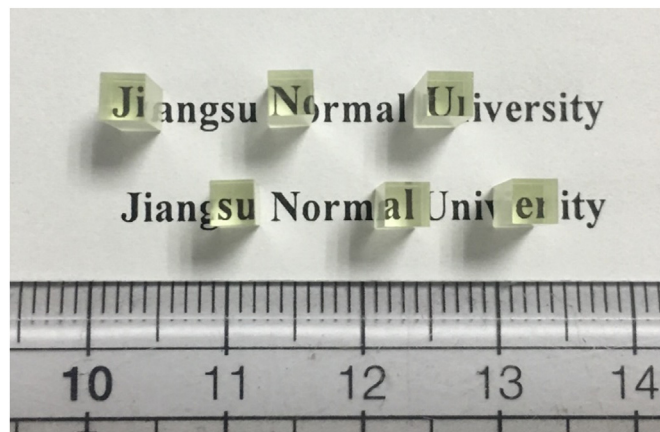


Fig. 1. Polished Sr_{0.5}La_{0.47}Pr_{0.03}Mg_{0.5}Al_{11.5}O₁₉ crystals used in the laser experiments.

polarizer was used to measure the polarized absorption and emission spectra. The polarized absorption spectra were measured with a UV–VIS–NIR spectrophotometer (Model Cary-5000, Varian, USA) at room temperature. The polarized fluorescence spectra and the decay curve at 642 nm were recorded by using Edinburgh Instruments FLS980 spectrophotometer under 444 nm excitation.

3. Spectroscopy

3.1. Absorption spectra

Fig. 2 presents the polarized absorption spectra of Pr:ASL crystal in the range from 400 to 2500 nm. Nine absorption bands were registered. The absorption bands are attributed to the transitions from the ground state ³H₄ to the excited states, as marked in Fig. 2. For σ -polarization and π -polarization, the absorption cross-sections are 1.06×10^{-20} cm² at 444 nm and 0.38×10^{-20} cm² at 471 nm, and the full width at half maximum (FWHM) are 11.5 nm and 7.7 nm, respectively. Such a large FWHM could decrease the requirement of temperature stability for pumping laser. Besides, the considerable absorption cross section peak at 444 nm suitable for commercially InGaN pumping is much close to those calculated previously for 5 at.% Pr:SRA crystal (1.3×10^{-20} cm² at 444.5 nm [27]) and 2 at.% Pr:ASL (1.3×10^{-20} cm² at 444 nm [31]), which shows the advantage in laser operation.

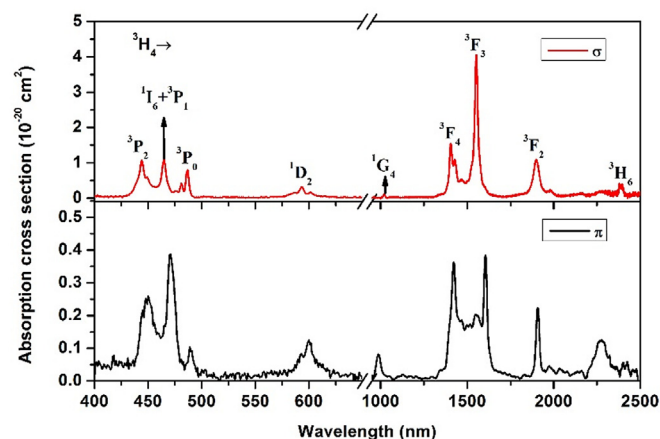


Fig. 2. Polarized absorption spectra of Pr:ASL crystal.

3.2. Judd-Ofelt analysis

In order to determine the radiative lifetime (τ_{rad}) of the $^3\text{P}_0$ multiplet, the Judd-Ofelt theory [38,39] was used to calculate the spectral parameters based on the polarized absorption spectra of Pr:ASL crystal. The obtained $\Omega_{2,4,6}$ values are shown in Table 1. The effective spectral parameters could be calculated according to the formula $\Omega_{\text{eff}} = (2\Omega_{\sigma} + \Omega_{\pi})/3$. The spectral parameters were applied to calculate the spontaneous emission probabilities A and fluorescence branching ratios β as given in Table 2. The average spontaneous emission probability were calculated by $A = (2A_{\sigma} + A_{\pi})/3$. Radiative lifetime of the $^3\text{P}_0$ level of Pr^{3+} ions in ASL crystal was calculated to be 59.5 μs , which is among the highest values for Pr^{3+} -doped oxide crystals.

3.3. Emission spectra

Under 444 nm exciting, the polarization-dependent emission spectra of Pr:ASL crystal were carried out. The emission cross sections are calculated by the Fuchtbauer-Ladenburg (F-L) formula, as shown in Fig. 3. From Fig. 3, it can be seen that four highest emission bands exist throughout the whole visible spectral region. These peaks positions are located at 487 nm ($^3\text{P}_0 \rightarrow ^3\text{H}_4$), 622 nm ($^3\text{P}_0 \rightarrow ^3\text{H}_6$), 646 nm ($^3\text{P}_0 \rightarrow ^3\text{F}_2$) and 727 nm ($^3\text{P}_0 \rightarrow ^3\text{F}_4$) with corresponding cross sections of 5.55×10^{-20} , 5.23×10^{-20} , 3.63×10^{-20} and $4.09 \times 10^{-20} \text{ cm}^2$ for σ polarization, respectively. The value of emission cross section at 487 nm is comparable with that of oxide host crystals such as 3 at.% Pr:LMA ($5.55 \times 10^{-20} \text{ cm}^2$ at 488 nm [30]) and 2 at.% Pr:ASL ($4.9 \times 10^{-20} \text{ cm}^2$ at 489 nm [31]), but lower than that of fluoride host crystals like 0.65 at.% Pr:YLF ($1.9 \times 10^{-19} \text{ cm}^2$ at 479 nm [40]) and 1.25 at.% BaY₂F₈ ($7.1 \times 10^{-20} \text{ cm}^2$ at 480 nm [41]). It is worth noting that comparatively broad FWHMs of 5.5 nm, 8.1 nm, 5.6 nm and 5.3 nm of emission peaks centered around 487 nm, 622 nm, 646 nm and 727 nm have been calculated, which could be favorable to realize tunable laser operation, as well as ultrashort pulses by mode locking.

3.4. Fluorescence lifetime

The fluorescence lifetime of the $^3\text{P}_0$ excited state was measured and shown in Fig. 4. The excitation wavelength and the monitoring wavelength were 444 nm and 642 nm, respectively. The decay curve exhibited a strictly single exponential behavior and the lifetime was calculated to be 39.6 μs . The fluorescence lifetime is smaller than the radiative lifetime. The J–O theory is a phenomenological theory but not a first-principles method [42]. Thus, the lifetime deviation from the experimental to theoretical data to a certain degree is understandable. The fluorescence lifetime is comparable with that of 1 at.% Pr:SRA (39.0 μs [27]), but much higher than that of 1 at.% Pr:ASL (37.3 μs [31]), 3 at.% Pr:ASL (36.1 μs [31]) and 3 at.% Pr:SRA (33.0 μs [27]). Even SRA crystal and ASL crystals with different La^{3+} composition have the same crystal structure, they provide Pr^{3+} ions different crystal field environment, which leads to different spectral property including lifetime of Pr^{3+} . The results indicate the potential of Pr:Sr_{0.5}La_{0.5}Mg_{0.5}Al_{11.5}O₁₉ crystal for visible laser generation.

Table 1
Judd-Ofelt intensity parameters of Pr:ASL crystal.

Intensity parameter	σ (10^{-20} cm^2)	π (10^{-20} cm^2)	Effective (10^{-20} cm^2)
Ω_2	1.069	0.348	0.829
Ω_4	2.980	0.791	2.250
Ω_6	7.950	1.552	5.817

Table 2

Calculated spontaneous emission probabilities, fluorescence branching ratios and radiative lifetime of Pr:ASL crystal.

Transition	A_{σ} (s^{-1})	A_{π} (s^{-1})	A (s^{-1})	β (%)	τ_r (μs)
$^3\text{P}_0 \rightarrow$					
$^3\text{H}_4$	11364.15	3047.89	8592.06	51.14	59.5
$^3\text{H}_6$	5980.04	468.26	4142.78	24.66	
$^3\text{F}_2$	2132.21	1523.67	1929.36	11.48	
$^3\text{F}_4$	2567.40	332.45	1822.42	10.85	
$^1\text{G}_4$	433.62	67.33	311.52	1.85	
$^1\text{D}_2$	1.23	6.73	3.06	0.02	

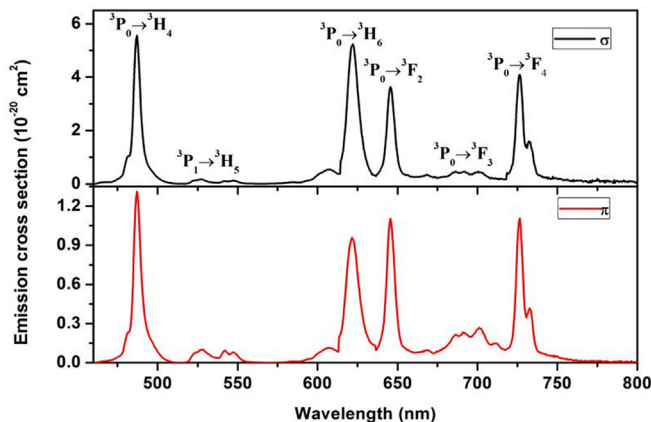


Fig. 3. Polarized emission spectra of Pr:ASL crystal.

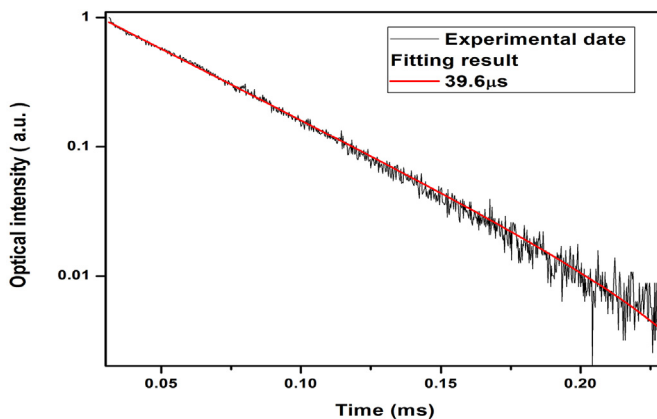


Fig. 4. The decay curve of the $^3\text{P}_0$ level of Pr:ASL crystal.

4. Laser properties

Laser experimental setup of the blue-diode-pumped continuous-wave Pr:ASL crystal lasers is shown schematically in Fig. 5. The pump source is an InGaN blue diode laser with maximum output power of about 2 W and emitting wavelength of about

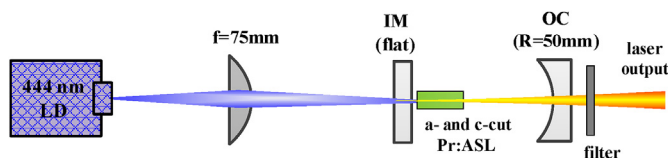


Fig. 5. The schematic of blue diode-pumped Pr:ASL laser experimental setup.

444 nm. The pump beam was focused by an aspherical plane-convex lens with focal length of 75 mm. The laser resonator was configured to be nearly hemispherical with cavity length of about 50 mm. The input mirror (IM) has a high transmission of about 90% at pump wavelength and high reflection of more than 99.9% at these considered wavelengths. Several output couplers (OCs) were used to explore the best laser performance with different transmissions. For deep red laser emission at about 726 nm, the transmissions of the four OCs at this wavelength are 0.98% (OC1), 2.45% (OC2), 3.29% (OC3) and 1.23% (OC4). For red laser emission at about 645 nm, transmission of the only one OC is 1.02%. All these OCs have curvature radii of 50 mm. Two laser gain media of Pr:ASL crystals, respectively cut along a and c crystalline axes, were used both with dopant concentrations of 3 at.% and dimensions of $3 \times 3 \times 10 \text{ mm}^3$. To protect the laser crystals from thermal fracturing, they were wrapped with indium foil to enhance the thermal contact and then mounted inside a copper block, which was connected to a chiller with temperature set at 14°C .

The experimental results of the a-cut sample are shown in Fig. 6. The output power curve shows that using the OC1 a maximum output power up to 92.8 mW was achieved with threshold of 250 mW of absorbed power, which led to a slope efficiency of about 11.9% by linear fit. Using OC2, the maximum output power decreased to 73.9 mW and the threshold increased to 393 mW. The corresponding slope efficiency was linearly fitted to be about 10.4%. Using OC3, the maximum output power further reduced to 69.3 mW with a slope efficiency of about 14.1%. The larger slope efficiency is because of the far higher threshold with OC3. Using OC4 for laser operation led to similar results to using OC1 with a maximum output power of 91.1 mW and slope efficiency of about 12.3%. From the output power curves in Fig. 6(a), one can find the output powers for all the curves display saturations more or less when the absorbed power exceeded to about 1100 mW. The saturation effect should be explained by thermal lensing effect inside the a-cut Pr:ASL crystal, which led to the laser resonator being operated at stability limit or even unstable any more. Under the four cases, i.e. four OCs, the laser wavelengths were monitored to be almost the same. Fig. 6(b) shows the laser wavelength registered at maximum output power with a peak at 726.1 nm. Beam quality of the 726.1 nm deep red laser at the maximum output power was appraised by measuring the output beam sizes at different locations, as shown in Fig. 6(c). By fitting the data to the expression of beam propagation factor M^2 , we estimated the M^2 to be about 1.61 and 1.22 in x and y directions. Adjusting the laser resonator by

slightly tilting the a-cut Pr:ASL or OCs for reshaping the output laser beam to be circular symmetry has led to power drop. Using a Glan-Taylor polarizer, we monitored these 726 nm laser emissions to be linearly polarized.

Red laser operation was also performed and the results are shown in Fig. 7. The maximum output power reached 49.2 mW and the threshold is about 399 mW. The corresponding slope efficiency is about 6.7%. The lasing wavelength peaks at 645.78 nm (see Fig. 7(b)), which is very similar to the lasing wavelength of Pr:KY₃F₁₀ crystal [16]. However, the red emission of the Pr:KY₃F₁₀ laser was unpolarized because of its isotropy, while the present 645.78 nm was measured to be linearly polarized. Note that, all these output laser emissions at deep red and red should be σ -polarized because of its larger emission cross section in this polarization according to Fig. 2. In addition, we measured the M^2 factor of the red laser to be about 1.48 and 1.10 in x and y directions (see Fig. 7(c)).

In the following, we report on the results in regard to c-cut Pr:ASL sample. Fig. 8 in the left plots the output power varying with absorbed power. Basically, comparing with the above investigation with a-cut sample, the four sets of power data show similar curves. Using OC1, the maximum output power reached 46.6 mW with threshold of 509 mW and the slope efficiency was found to be about 8.0%. Using OC2, OC3 and OC4, the maximum output power changed to 33.4 mW, 31.5 mW and 42.8 mW, while the corresponding slope efficiencies became 8.6%, 9.8% and 8.2%, respectively. At maximum, the peak wavelength was measured to be 725.9 nm (see Fig. 8(b)), i.e. about 0.2 nm shift from the case with a-cut sample. Since the measuring precision of the wavelength meter is about 0.2 nm, we cannot determine whether this shift is real. Again, the output laser beam was measured to have M^2 factor of 1.74 and 1.56 in x and y directions (see Fig. 8(c)). Moreover, using the same device, we found that the 725.9 nm deep red lasers show no polarization, which is reasonable considering the c-cut sample.

Results of the red laser emission using the c-cut sample are shown in Fig. 9. The threshold is about 510 mW and the maximum output power is 42.8 mW. It gives a slope efficiency of about 8.5%. The lasing wavelength peaks at 646.04 nm at maximum output power. The laser beam quality was measured to be about 1.79 and 1.27 in x and y direction. No polarization effect of the red laser emission was found. Compared with Ref. [31], the present laser is still potential in scaling the power and efficiency by optimizing the quality of the Pr:ASL crystal, which will be our next investigation in the near future.

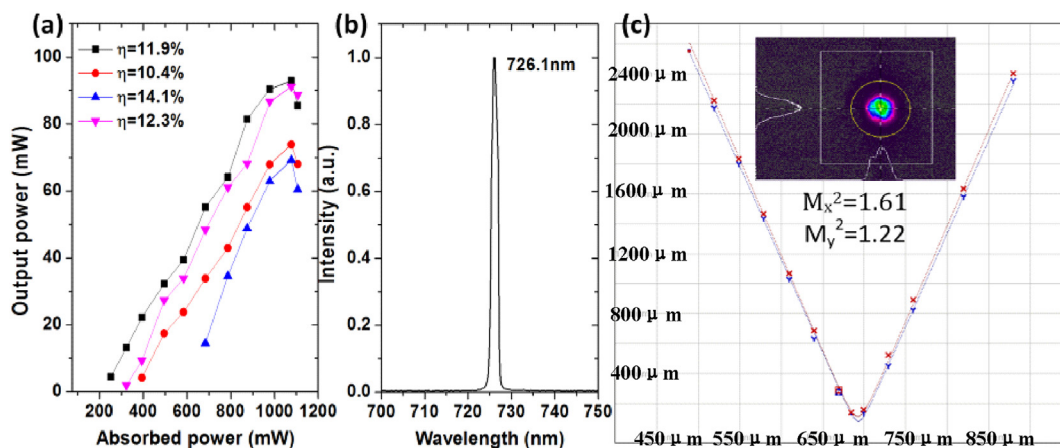


Fig. 6. (a) The dependence of output power on absorbed power of a-cut Pr:ASL laser at deep red, (b) the corresponding laser spectrum with peak at 726.10 nm and (c) Beam spot sizes of the 726.10 nm laser at different distances at maximum output power; inset: the spot image. (For interpretation of the references to color in this figure legend, the reader is referred to the Web version of this article.)

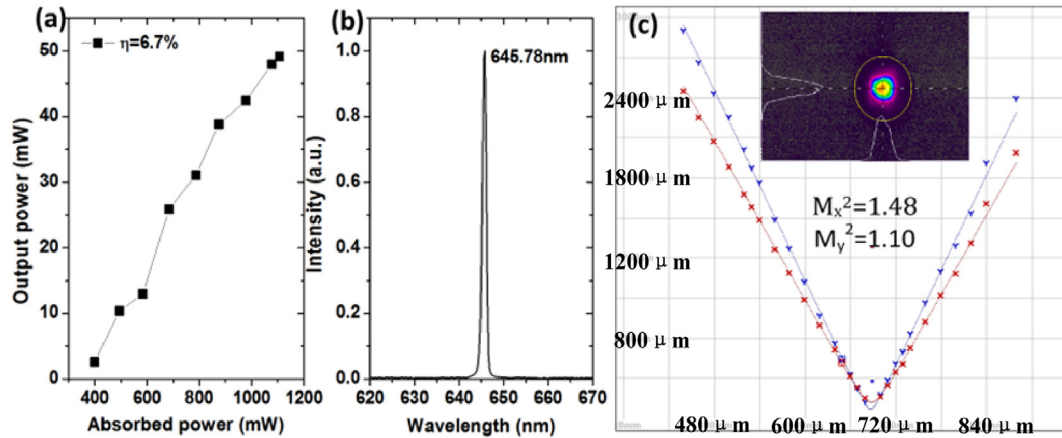


Fig. 7. (a) The dependence of output power on absorbed power of a-cut Pr:ASL laser at red, (b) the corresponding laser spectrum with peak at 645.78 nm and (c) Beam spot sizes of the 645.78 nm laser at different distances at maximum output power; inset: the spot image. (For interpretation of the references to color in this figure legend, the reader is referred to the Web version of this article.)

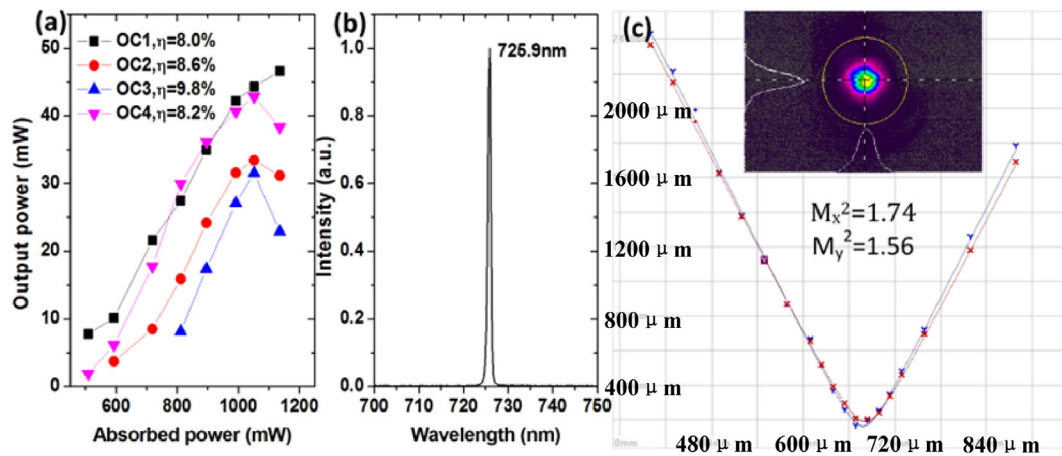


Fig. 8. (a) The dependence of output power on absorbed power of c-cut Pr:ASL laser at deep red, (b) the corresponding laser spectrum with peak at 725.90 nm and (c) Beam spot sizes of the 725.90 nm laser at different distances at maximum output power; inset: the spot image. (For interpretation of the references to color in this figure legend, the reader is referred to the Web version of this article.)

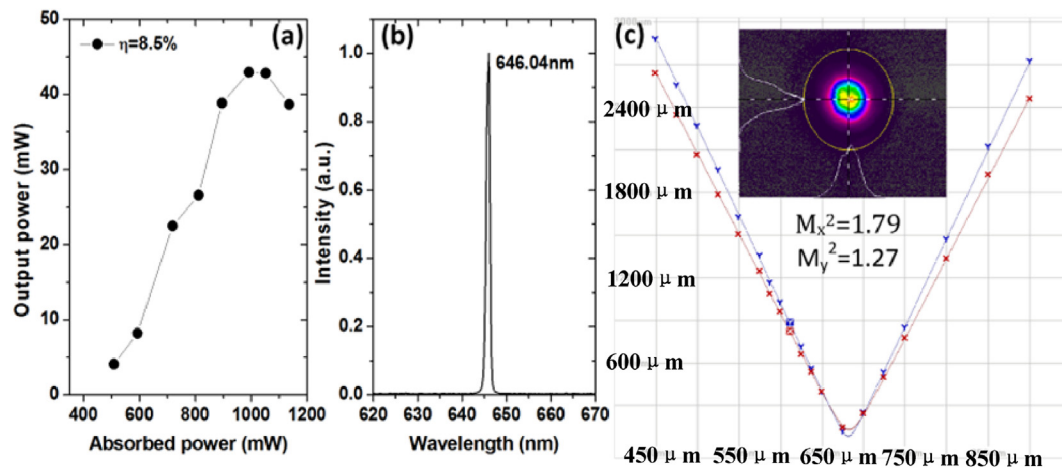


Fig. 9. (a) The dependence of output power on absorbed power of c-cut Pr:ASL laser at red, (b) the corresponding laser spectrum with peak at 646.04 nm and (c) Beam spot sizes of the 646.04 nm laser at different distances at maximum output power; inset: the spot image. (For interpretation of the references to color in this figure legend, the reader is referred to the Web version of this article.)

5. Conclusions

In conclusion, Pr:ASL crystal has been grown using the Czochralski method. Absorption and emission spectra of Pr:ASL crystal were measured for corresponding calculations of cross sections. Continuous-wave laser operation of the a- and c-cut samples under InGaN laser diode pumping has been demonstrated. For deep red laser at about 726 nm, the maximum output powers achieved from a-cut sample is 92.8 mW with slope efficiency of about 11.9%, while 46.6 mW with slope efficiency of 8.0% for c-cut sample. For red laser at about 645 nm, maximum output powers of 49.2 mW and 42.8 mW were obtained for the a-cut sample and c-cut sample, corresponding to a slope efficiency of 6.7% and 8.5%, respectively. Improving the laser performance could be realized by optimizing the quality of the Pr:ASL crystal.

Acknowledgements

This work is partially supported by National Key Research and Development Program of China (No. 2016YFB0701002), National Natural Science Foundation of China (No. 61621001, 61605069), Natural Science Foundation of Fujian Province of China (2018J01108) and Principal fund of Xiamen University (20720180082).

References

- [1] C. Kränkel, D.-T. Marzahl, F. Moglia, G. Huber, P.W. Metz, Out of the blue: semiconductor laser pumped visible rare-earth doped lasers, *Laser Photon. Rev.* 10 (2016) 548–568.
- [2] H.J. Chen, P. Loiseau, G. Aka, C. Kränkel, Optical spectroscopic investigation of $\text{Ba}_3\text{Tb}(\text{PO}_4)_3$ single crystals for visible laser applications, *J. Alloys Compd.* 740 (2018) 1133–1139.
- [3] G. Gheorghie, S. Hau, L. Gheorghie, F. Voicu, M. Greculeasa, M. Enculescu, K.M. Belikov, E.Yu. Bryleva, O.V. Gaiduk, Yellow laser potential of cubic $\text{Ca}_3(\text{Nb,Ga})_5\text{O}_{12}:\text{Dy}^{3+}$ and $\text{Ca}_3(\text{Li,Nb,Ga})_3\text{O}_{12}:\text{Dy}^{3+}$ single crystals, *J. Alloys Compd.* 739 (2018) 806–816.
- [4] Y.X. Zhang, D.Z. Lu, H.H. Yu, H.J. Zhang, Low-dimensional saturable absorbers in the visible spectral region, *Adv. Opt. Mater.* 7 (2019), 1800886.
- [5] Y.F. Chen, Y.C. Liu, Y.Y. Pan, D.Y. Gu, H.P. Cheng, C.H. Tsou, H.C. Liang, Efficient high-power dual-wavelength lime-green Nd:YVO₄ lasers, *Opt. Lett.* 44 (2019) 1323–1326.
- [6] H.X. Fan, Y. Chen, T. Yan, J. Lin, G. Peng, J.Y. Wang, R.I. Boughton, N. Ye, Crystal growth, spectral properties and Judd-Ofelt analysis of $\text{Pr}^{3+}:\text{LaMgAl}_{11}\text{O}_{19}$, *J. Alloys Compd.* 767 (2018) 938–943.
- [7] Y. Xiao, M. Ju, X.Y. Kuang, X.Y. Yeung, A systematic study of the microstructure and laser characteristics of Pr^{3+} -doped lithium lutetium fluoride, *J. Alloys Compd.* 749 (2018) 391–398.
- [8] H. Yu, X.B. Qian, L.Y. Guo, D.P. Jiang, Q.H. Wu, F. Tang, L.B. Su, Q.W. Ju, J.Y. Wang, J. Xu, Pr:Ca_{1-x}R_xF_{2+x} (R=Y or Gd) crystals: modulated blue, orange and red emission spectra with the properties of R^{3+} ions, *Opt. Mater.* 78 (2018) 88–93.
- [9] Q.Q. Hu, Z.T. Jia, S. Veronesi, J. Zhang, A. Sottile, M. Tonelli, E. Cavalli, X.T. Tao, Crystal growth and optimization of Pr:CaGdAlO₄ by the flux Czochralski method, *CrystEngComm* 20 (2018) 590–596.
- [10] G.Q. Yi, W.W. Li, J.H. Song, B.C. Mei, Z.W. Zhou, L.B. Su, Preparation and characterizations of $\text{Pr}^{3+}:\text{CaF}_2$ transparent ceramics with different doping concentrations, *Ceram. Int.* 45 (2019) 3541–3546.
- [11] V. Hegde, C.S.D. Viswanath, N. Chauhan, K.K. Mahato, S.D. Kamath, Photoluminescence and thermally stimulated luminescence properties of Pr^{3+} -doped zinc sodium bismuth borate glasses, *Opt. Mater.* 84 (2018) 268–277.
- [12] C.A.S. Flizikowski, V.S. Zanuto, L.A.O. Nunes, M.L. Baesso, L.C. Malacarne, N.G.C. Astrath, Standard and modified Judd-Ofelt theories in Pr^{3+} -doped calcium aluminosilicate glasses: a comparative analysis, *J. Alloys Compd.* 780 (2019) 705–710.
- [13] H. Tanaka, S. Fujita, F. Kannari, High-power visibly emitting $\text{Pr}^{3+}:\text{YLF}$ laser end pumped by single-emitter or fiber-coupled GaN blue laser diodes, *Appl. Opt.* 57 (2018) 5923–5928.
- [14] Q. Yang, Y.P. Cao, X.Q. Liu, X.L. Lun, P.C. Wang, X.Y. Wang, Passive Q-switching of Pr:LiYF₄ visible laser using SnS₂ as a saturable absorber, *Optic Laser. Technol.* 112 (2019) 183–187.
- [15] B. Xu, P. Camy, J.L. Doualan, Z.P. Cai, R. Moncorgé, Visible laser operation of Pr^{3+} -doped fluoride crystals pumped by a 469 nm blue laser, *Optic Express* 19 (2011) 1191–1197.
- [16] J. Shu, E. Damiano, A. Sottile, Z.H. Zhang, M. Tonelli, Growth by the $\mu\text{-PD}$ method and visible laser operation of a single-crystal fiber of $\text{Pr}^{3+}:\text{KY}_3\text{O}_{10}$, *Crystals* 7 (2017) 200.
- [17] D. Pabœuf, O. Mhibik, F. Bretenaker, P. Goldner, D. Parisi, M. Tonelli, Diode-pumped Pr:BaY₂F₈ continuous-wave orange laser, *Opt. Lett.* 36 (2011) 280–282.
- [18] A. Sottile, Z.H. Zhang, S. Veronesi, D. Parisi, A. Di Lieto, M. Tonelli, Visible laser operation in a $\text{Pr}^{3+}:\text{LiLuF}_4$ monocryalline fiber grown by the micro-pulling-down method, *Opt. Mater. Express* 6 (2016) 1964–1972.
- [19] Y.X. Zhang, S.X. Wang, A. Di Lieto, G.L. Yu, H.H. Yu, H.J. Zhang, M. Tonelli, X.G. Xu, J.Y. Wang, Temperature-dependent fluorescence properties and diode-pumped deep red laser performance of Pr:LiGdF₄ crystal, *Chin. Phys. Lett.* 32 (2015), 054210.
- [20] B. Xu, F. Starecki, D. Pabœuf, P. Camy, J.L. Doualan, Z.P. Cai, A. Braud, R. Moncorgé, Ph. Goldner, F. Bretenaker, Red and orange laser operation of Pr:KYF₄ pumped by a Nd:YAG/LBO laser at 469.1 nm and a InGaN laser diode at 444 nm, *Optic Express* 21 (2013) 5567–5574.
- [21] A. Sottile, E. Damiano, M. Tonelli, Diode-pumped laser operation of $\text{Pr}^{3+}:\text{Ba}(\text{Y}_{0.8}\text{Lu}_{0.2})_2\text{F}_8$ in the visible region, *Opt. Lett.* 41 (2016) 5555–5558.
- [22] H. Yu, D. Jiang, F. Tang, L.B. Su, S.Y. Luo, X.G. Yan, B. Xu, Z.P. Cai, J.Y. Wang, Q.W. Ju, J. Xu, Enhanced photoluminescence and initial red laser operation in Pr:CaF₂ crystal via co-doping Gd^{3+} ions, *Mater. Lett.* 206 (2017) 140–142.
- [23] W.W. Ma, L.B. Su, X.D. Xu, J.Y. Wang, D.P. Jiang, L.H. Zheng, J.J. Liu, X.W. Fan, J. Liu, J. Xu, Improved 2.79 μm continuous-wave laser performance from a diode-end pumped Er,Pr:CaF₂ crystal, *J. Alloys Compd.* 695 (2017) 3370–3375.
- [24] W.W. Li, H.J. Huang, B.C. Mei, J.H. Song, X.D. Xu, Effect of Y^{3+} ion doping on the microstructure, transmittance and thermal properties of CaF₂ transparent ceramics, *J. Alloys Compd.* 747 (2018) 359–365.
- [25] M. Fibrich, H. Jelinkova, J. Sulc, K. Nejezchleb, V. Skoda, Pr:YAlO₃ microchip laser at 662 nm, *Laser Phys. Lett.* 8 (2011) 116–119.
- [26] X.J. Lin, X.X. Huang, B. Liu, B. Xu, H.Y. Xu, Z.P. Cai, X.D. Xu, D.Z. Li, J. Liu, J. Xu, Continuous-wave laser operation at 743 and 753 nm based on a diode pumped c-cut Pr:YAlO₃ crystal, *Opt. Mater.* 76 (2018) 16–20.
- [27] M. Fechner, F. Reichert, N.O. Hansen, K. Petermann, G. Huber, Crystal growth, spectroscopy, and diode pumped laser performance of Pr, Mg: SrAl₁₂O₁₉, *Appl. Phys. B* 102 (2011) 731–735.
- [28] A. Voss, F. Reichert, P.W. Metz, D.-T. Marzahl, C. Kränkel, G. Huber, T. Graf, Thin-disk laser operation of $\text{Pr}^{3+}, \text{Mg}^{2+}:\text{SrAl}_{12}\text{O}_{19}$, *Opt. Lett.* 39 (2014) 1322–1325.
- [29] F. Reichert, D.-T. Marzahl, G. Huber, Spectroscopic characterization and laser performance of Pr,Mg:CaAl₁₂O₁₉, *J. Opt. Soc. Am. B* 31 (2014) 349–354.
- [30] S.D. Zhou, Y.X. Pan, N. Li, B. Xu, J. Liu, Q.S. Song, J. Liu, D.Z. Li, P. Liu, X.D. Xu, J. Xu, Spectroscopy and diode-pumped laser operation of Pr:LaMgAl₁₁O₁₉ crystal, *Opt. Mater.* 89 (2019) 14–17.
- [31] S. Sattayaporn, P. Loiseau, G. Aka, D.T. Marzahl, C. Kränkel, Crystal growth, spectroscopy and laser performances of $\text{Pr}^{3+}:\text{Sr}_{0.7}\text{La}_{0.3}\text{Mg}_{0.3}\text{Al}_{11.7}\text{O}_{19}$ (Pr:ASL), *Optic Express* 26 (2018) 1278–1289.
- [32] L.D. Merkle, B. Zandi, R. Moncorgé, Y. Guyot, H.R. Verdun, B. McIntosh, Spectroscopy and laser operation of Pr,Mg: SrAl₁₂O₁₉, *J. Appl. Phys.* 79 (1996) 1849–1856.
- [33] H.R. Verdun, D.E. Wortman, C.A. Morrison, J.L. Bradshaw, Optical properties of Nd^{3+} in single crystal SrAl₁₂O₁₉, *Opt. Mater.* 7 (1997) 117–128.
- [34] C. Gheorghie, L. Gheorghie, A. Achim, S. Hau, R.D. Avram, G. Stanciu, Optical properties of Sm^{3+} doped strontium hexa-aluminate single crystals, *J. Alloys Compd.* 622 (2015) 296–302.
- [35] P. Xu, C.T. Xia, J.Q. Di, X.D. Xu, Q.L. Sai, L.L. Wang, Growth and optical properties of Co,Nd:LaMgAl₁₁O₁₉, *J. Cryst. Growth* 361 (2012) 11–15.
- [36] D.-T. Marzahl, P.W. Metz, C. Kränkel, G. Huber, Spectroscopy and laser operation of Sm^{3+} -doped lithium lutetium tetrafluoride (LiLuF₄) and strontium hexaaluminate (SrAl₁₂O₁₉), *Optic Express* 23 (2015) 21118–21127.
- [37] Y.X. Pan, S.D. Zhou, J.W. Wang, B. Xu, J. Liu, Q.S. Song, J. Xu, D.Z. Li, P. Liu, X.D. Xu, J. Xu, Growth, spectral properties, and diode-pumped laser operation of a Nd^{3+} -doped LaMgAl₁₁O₁₉ crystal, *Appl. Opt.* 57 (2018) 9657–9661.
- [38] B.R. Judd, Optical absorption intensities of rare-earth ions, *Phys. Rev.* 127 (1962) 750–761.
- [39] G.S. Ofelt, Intensities of crystal spectra of rare-earth ions, *J. Chem. Phys.* 37 (1962) 511–520.
- [40] A. Richter, E. Heumann, G. Huber, V. Ostroumov, W. Seelert, Power scaling of semiconductor laser pumped praseodymium-lasers, *Optic Express* 15 (2007) 5172–5178.
- [41] R. Hakim, K. Damak, A. Toncelli, M. Fourati, R. Maalej, Growth, optical spectroscopy and Judd-Ofelt analysis of Pr-doped BaY₂F₈ monocryalline, *J. Lumin.* 143 (2013) 233–240.
- [42] Y.Q. Zhang, B.J. Chen, S. Xu, X.P. Li, J.S. Zhang, J.S. Sun, X.Q. Zhang, H.P. Xia, R.N. Hua, A universal approach for calculating the Judd-Ofelt parameters of RE^{3+} in powdered phosphors and its application for the $\text{B-NaYF}_4:\text{Er}^{3+}/\text{Yb}^{3+}$ phosphor derived from auto-combustion-assisted fluoridation, *Phys. Chem. Chem. Phys.* 20 (2018) 15876–15883.